Research Article | Vol. 32, No. 7 / 25 Mar 2024 / Optics Express 12213

Optics EXPRESS

Circular quantum wire symmetrically loaded with a graphene strip as the plasmonic micro/nano laser: threshold conditions analysis

MSTYSLAV E. KALIBERDA,[1,*] SERGEY A. POGARSKY,[1] OLEKSII V. KOSTENKO,[2] OLEKSANDR I. NOSYCH,[3] AND TATIANA L. ZINENKO[3]

[1] School of Radiophysics, Biomedical Electronics and Computer Systems, V.N. Karazin Kharkiv National University, Kharkiv, Ukraine
[2] Department of Differential Equations, B. Verkin Institute of Low Temperature Physics and Engineering NASU, Kharkiv, Ukraine
[3] Laboratory of Micro and Nano Optics, O. Y. Usikov Institute of Radio-Physics and Electronics NASU, Kharkiv, Ukraine
[*] KaliberdaME@gmail.com

Abstract: We study, apparently for the first time, the threshold conditions for the time-harmonic natural modes of the micro-to-nanosize plasmonic laser shaped as a circular quantum wire with a flat graphene strip, placed symmetrically inside it, in the H-polarization case. We suppose that the quantum wire is made of a nonmagnetic gain material, characterized with the aid of the "active" imaginary part of the complex refractive index. The emergence of lasers integrating plasmonic effects marks a significant trend in contemporary photonics. Here, the graphene offers a promising alternative to the noble metals as it exhibits the capacity to sustain plasmon-polariton natural surface waves across the infrared and terahertz (THz) spectra. The used innovative approach is the lasing eigenvalue problem (LEP), which is classical electromagnetic field boundary-value problem, adapted to the presence of active region. It is tailored to deliver both the mode-specific emission frequency, which is purely real at the threshold, and the value of the gain index of the active region, necessary to make the frequency real-valued. The conductivity of graphene is characterized using the quantum Kubo formalism. We reduce the LEP for the considered nanolaser to a hyper-singular integral equation for the current on the strip and discretize it by the Nystrom-type method. This method is meshless and computationally economic. After discretization, a matrix equation is obtained. The sought for mode-specific pairs {the frequency and the threshold gain index} correspond to the zeros of the matrix determinant. It should be noted that the convergence to exact LEP eigenvalues is guaranteed mathematically if the discretization order is taken progressively larger. Two families of modes are identified and studied: the modes of the quantum wire, perturbed by the presence of the graphene strip and the plasmon modes of the strip. The frequencies of all plasmon modes and the lowest mode of the quantum wire are found to be well-tuned by changing the chemical potential of graphene. Engineering analytic formulas for the plasmon-mode frequencies and thresholds are derived. We believe that the presented results can be used in the creation of single-mode tunable micro and nanolasers.

1. Introduction

The development of lasers that incorporate plasmonic effects represents a promising trend in modern photonics [1]. Nanowire lasers, proposed in [2–6], exemplify the ongoing trends towards miniaturization. A pivotal advancement in scaling down the size of lasers came with the introduction of noble-metal based nanoparticles as open cavities operating on the plasmon

#514643 https://doi.org/10.1364/OE.514643
Journal © 2024 Received 28 Nov 2023; revised 23 Feb 2024; accepted 4 Mar 2024; published 19 Mar 2024

Optics EXPRESS

modes [7]. The first plasmonic nanolasers, a.k.a. spasers, were experimentally demonstrated in [8–10]. Subsequently, this category of nanolasers underwent extensive development and refinement [11–15].

A sheet of graphene, a revolutionary 2D material, has the capability to support plasmon-polariton natural surface wave in both the infrared and THz ranges [16,17]. If graphene is patterned, for instance, as a strip of finite width, then it forms an open resonator, where the natural modes are generated by the plasmon wave, reflected from the strip edges. What is especially attractive for applications, the graphene conductivity and hence the plasmon mode frequencies can be dynamically controlled through the application of electrostatic or magnetostatic bias. Graphene conductivity σ is a function of the frequency f, chemical potential μ_c, electron relaxation time τ and temperature T, $\sigma = \sigma(f, \mu_c, \tau, T)$. It can be obtained from the Kubo formalism [16,17]. The dynamic control of graphene's conductivity offers significant flexibility in tailoring the behavior of graphene-based devices, including sensors, absorbers, and antennas [18–22]. It is natural to suggest that patterned graphene can replace noble-metal particle and serve as a resonance element of plasmonic nanolaser [23,24]. Here, graphene's tunability has the potential to enable control over emission frequency and threshold, opening up exciting possibilities for tunable laser emission. Taking into account that graphene is able to support surface plasmon polariton waves at much lower frequencies than noble metals, its application can downshift the operation range of the plasmonic nanolasers.

From the viewpoint of computational electromagnetics, "atomic" thickness of graphene allows assuming it to have zero thickness and characterizing with the aid of resistive-sheet boundary conditions [16]. Note that these conditions are more complicated than those for the perfect electrical conductor (PEC), however, they turn to the latter if the conductivity tends to infinity. The resistivity of graphene is also called the surface impedance; it is the inverse of the complex-valued surface conductivity given by the Kubo formulas. Here, it is worth noting that sometimes graphene is characterized with the aid of effective dielectric permittivity, which is taken as Kubo's surface conductivity divided by the empirically selected thickness (usually 1-2 nm) [21].

To address the eigenvalue electromagnetic field problem (i.e. without external sources) from the viewpoint of lasing threshold, we will use the LEP approach. This approach is custom-designed to provide the real-valued modal frequencies and the corresponding values of the gain index in the active region, necessary to make the eigenfrequency of open cavity real-valued. Here, the vanishing of the imaginary part of the eigenfrequency is identified with the threshold of stationary emission; moreover, it was shown in [25] that this is equivalent to the classical definition of threshold as "total loss = total gain" condition. Unlike the conventional eigenvalue problem based on the Q-factor theory for a passive optical cavity, LEP takes into account the active region's size, shape, and position in comprehensive manner. This enables using the active-region geometry as engineering parameter to manipulate the gain-index threshold value via controlling the overlap between the mode electric field pattern and the active region [25].

At first, the LEP formalism was successfully applied to study the threshold conditions of various microcavity laser configurations, fully or partially filled in with gain material [26–29]. Later, it was used to analyze the modes of the noble-metal nanolasers, namely, a silver strip [30] and a silver tube [31] inside the circular quantum wire (QWR) as active region. More recently, the threshold conditions for the modes of nanolasers composed of a single and a pair of graphene-covered circular QWRs were studied in [32,33]. The mode-specific threshold analysis helps determine the minimum pump power required to initiate lasing action. By understanding the threshold conditions, one can optimize the laser design and parameters to achieve efficient operation. Together with the emission frequency analysis, such study shows how to achieve the single-mode operation by manipulating either the pump level or the gain frequency envelope. Besides, the quantum dots and wires often exhibit blinking, characterized by erratic luminosity

Optics EXPRESS

caused by random fluctuations. However, employing a resonant element can effectively stabilize quantum wires, mitigating the blinking phenomena [34].

In this paper, we consider the circular QWR of non-magnetic gain material, equipped with flat graphene strip located in the QWR center – see Fig. 1.

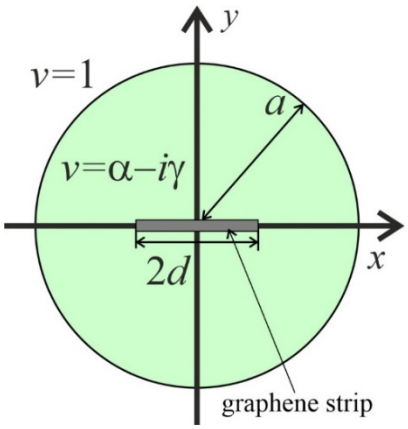

Fig. 1. Cross-sectional geometry of the circular QWR with the zero-thickness graphene strip inside.

2. Modified eigenvalue problem statement

The cross-section of a circular QWR of the radius a, loaded with a zero-thickness graphene strip of the width $2d$, is shown in Fig. 1. The wire axis is co-located with the strip middle line and coincides with the z-axes of Cartesian (x,y,z) and cylindrical (r,ϕ,z) coordinates. The material of the wire is characterized by the complex refractive index, $v = \alpha - i\gamma$. We suppose that the QWR consists of the gain material, so that $\alpha>0$, $\gamma>0$. The structure is infinite along the z-axis that allows considering two orthogonal polarizations of the electromagnetic field separately. We consider the H- polarization case (magnetic field vector is parallel to the z -axis), since the plasmon modes of the graphene strip are known to be absent in the E -polarization case. The time dependence $exp(-i\omega t)$ is assumed and omitted.

The H-polarized field can be conveniently characterized with the aid of the z-component of magnetic field. This component has to satisfy a two-dimensional (2-D) boundary-value problem in the laser cross-section for the Helmholtz equation with wavenumber $k = \omega/c$ (where c is the light velocity) out of QWR and $k_1 = kv$ inside QWR. This problem has the following set of the boundary conditions: the resistive-sheet conditions at the graphene strip,

$$E_y^+ = \frac{1}{\sigma}(H_z^+ - H_z^-),\ |x|<d,\ y = 0, \tag{1}$$

$$E_y^+ = E_y^-,\ |x|<d,\ y = 0, \tag{2}$$

the tangential component continuity conditions at the QWR boundary,

$$E_y^+ = E_y^-,\ r = a,\ \phi \in [0, 2\pi), \tag{3}$$

$$H_z^+ = H_z^-,\ \phi \in [0, 2\pi), \tag{4}$$

where symbols "±" denote the limit values of the field components above (for "+") or below (for "−") the interfaces, the Sommerfeld radiation condition at the infinity,

$$\frac{\partial H_z}{\partial r} - ikH_z = o\left(\frac{1}{\sqrt{r}}\right),\ r \to \infty, \tag{5}$$

Optics EXPRESS

where r is the distance, and the local power finiteness condition (the edge condition),

$$\int_\Omega (|H_z|^2 + |kZ_0 \nabla H_z|^2) ds < \infty, \tag{6}$$

where $\Omega \subset R^2$ is an arbitrary domain and $Z_0 = 120\pi\Omega$ is the free-space impedance. In the case of zero thickness graphene strip, Eq. (6) is equivalent to $H_z = O\left(\sqrt{\rho}\right)$ and $|\nabla H_z| = O\left(1/\sqrt{\rho}\right)$, if the distance to the edge $\rho \to 0$.

These conditions are inherited from the classical real-frequency wave-scattering problems where they are satisfied by the residues in the real-frequency poles of the scattered field functions.

The formulated above problem has no given sources or incident field. Instead, we assume that the geometrical parameters and the active region refractive index, α, are given, and look for the eigenvalue pairs, (f, γ), which generate non-zero functions H_z that satisfy the problem conditions.

3. Casting the eigenvalue problem to determinantal equations

The considered nanolaser configuration has two components. One of them is graphene strip and the other is QWR of the circular cross-section. To reduce the stated above LEP to determinantal equation, we introduce the electric current density function on the strip as $w(x) = H_z^+(x, y) - H_z^-(x, y)$, $|x| < d$, $y = 0$. Then, following [30], we present unknown field function H_z as a double-layer potential, i.e. convolution of the current with the normal derivative of the circular dielectric rod Green's function $G(\vec{r}, \vec{r}_1)$,

$$H_z(\vec{r}) = \int_{-d}^{d} w_n(x_1) \frac{\partial G(\vec{r}, \vec{r}_1)}{\partial y_1} dx_1, \quad y_1 = 0, \tag{7}$$

where $\vec{r} = (x, y)$ is the radius-vector of the observation point, $\vec{r}_1$ is the radius-vector of the point on the strip. Here, the Green's function complies with the radiation condition (5).

Thanks to linear character of the integral operator, function (7) automatically satisfies the boundary conditions at the QWR contour and the radiation condition at infinity (5). The dielectric rod Green's function has two arguments, $\vec{r}_1$ and $\vec{r}$, which can correspond to the inner and outer domains of QWR. However, Eq. (7) implies that both $\vec{r}_1$ and $\vec{r}$ are inside QWR. Then the Green's function can be represented as a sum of two terms [30],

$$G(\vec{r}, \vec{r}_1) = \begin{cases} G_0(\vec{r}, \vec{r}_1) + G_1(\vec{r}, \vec{r}_1), r < a, \\ G_1(\vec{r}, \vec{r}_1), r > a, \end{cases} \tag{8}$$

where G_0 is the Green's function of the 2-D space filled in with the same material as QWR,

$$G_0(\vec{r}, \vec{r}_1) = \frac{i}{4} H_0(k_1 |\vec{r} - \vec{r}_1|), \tag{9}$$

and G_1 accounts for the presence of the dielectric rod. Using the separation of variables, the latter function can be derived in explicit form, as Fourier series in terms of the angular exponents,

$$G_1(\vec{r}, \vec{r}_1) =$$

$$\begin{cases} -\frac{1}{4} \sum_{m=-\infty}^{\infty} A_m J_m(k_1 r) J_m(k_1 r_1) \sin m\phi exp(\, im\phi_1), r < a, \\ -\frac{1}{4} \sum_{m=-\infty}^{\infty} B_m H_m(kr) J_m(kr_1) \sin m\phi exp(\, im\phi_1), r > a, \end{cases} \tag{10}$$

$$A_m = (H_m(ka) H'_m(k_1 a)/v - H'_m(ka) H_m(k_1 a))/C_m, \tag{11}$$

$$B_m = 2i/(\pi k_1 a C_m v), \tag{12}$$

$$C_m = J_m(k_1 a) H'_m(ka) - J'_m(k_1 a) H_m(ka)/v, \tag{13}$$

where $J_m(\cdot)$ and $H_m(\cdot)$ are the Bessel and Hankel (first kind) functions, and the prime stands for the differentiation in the argument.

Optics EXPRESS

Now, on using Eq. (2), substituting Eq. (7) into Eq. (1), and taking into account the limit values of the double-layer potential, we obtain the following boundary integral equation:

$$\begin{aligned} &4k_1 vZw(x) + k_1 \int_{-d}^{d} \frac{H_1(k_1|x-x_1|)}{|x-x_1|} w(x_1)dx_1 + \int_{-d}^{d} \sum_{m=-\infty}^{\infty} C_m m^2 \\ &\times \mathrm{sgn}(x^{m-1}x_1^{m-1}) J_m(k_1|x|)J_m(k_1|x_1|)/|xx_1|w(x_1)dx_1 = 0,\ |x|<d, \end{aligned} \tag{14}$$

where $Z = (\sigma Z_0)^{-1}$ is the surface impedance of graphene, normalized by the free-space impedance, Z_0.

Note that, according to the edge condition, the current density tends to zero at the edges of the strip,

$$w(x) \sim \sqrt{d^2 - x^2}, x \to \pm d. \tag{15}$$

The integrand of the first integral in Eq. (14) contains a second order-singularity and should be understood in the sense of the Hadamar finite part. Considering Eq. (15), after transforming the integration interval $(-d; d)$ to a standard one $(-1; 1)$, we rewrite Eq. (14) as follows:

$$\begin{aligned} &4k_1 vZ\tilde{w}(t)\sqrt{1-t^2} - \frac{2i}{\pi d} \int_{-1}^{1} \frac{1}{|t-t_1|^2} \tilde{w}(t_1)\sqrt{1-t_1^2}dt_1 \\ &+k_1 i \int_{-1}^{1} \ln|t-t_1|\tilde{w}(t_1)\sqrt{1-t_1^2}dt_1 + \int_{-1}^{1} F(t,t_1)\tilde{w}(t_1)\sqrt{1-t_1^2}dt_1 = 0, \end{aligned} \tag{16}$$

where $t = x/d$, $t_1 = x_1/d$, $F(t, t_1)$ is regular function without the singularities for $t, t_1 \in (-1; 1)$, $w(x) = \tilde{w}(t)\sqrt{1-t^2}$.

Further, we use the Gauss-Chebyshev quadrature rule with the weight $\sqrt{1-t^2}$ for the discretization of (16). Here, the zeros of the Chebyshev polynomials of the second kind, $t_l = \cos(\pi l/N)$, $l = 1, \ldots, N$, serve as both interpolation and collocation points, and N is the order of the discretization scheme. Following the same lines as in [30], we obtain a homogeneous matrix equation with matrix $A^{(N)}$ of the finite order N,

$$\begin{aligned} &4k_1 vZ\tilde{w}(t_l)\sqrt{1-t_l^2} - \frac{2i}{\pi d} \sum_{j=1}^{N} C_{1,l,j}\tilde{w}(t_j) \\ &+k_1 i \sum_{j=1}^{N} C_{2,l,j}\tilde{w}(t_j) + k_1 i \sum_{j=1}^{N} C_{3,j}F(t_l,t_j)\tilde{w}(t_j) = 0,\ l = 1, \ldots, N, \end{aligned} \tag{17}$$

where $C_{1,l,j}$, $C_{2,l,j}$, and $C_{3,j}$ are coefficients of the quadrature rule for the hyper-singular integrals, integrals with logarithmic singularity, and regular integrals. Then, the sought pairs (f, γ) are the solutions of the determinant equation,

$$detA^{(N)}(f, \gamma) = 0. \tag{18}$$

To solve Eq. (18), we use the gradient-descent method [35], based on the iterative equation

$$\begin{pmatrix} f^j \\ \gamma^j \end{pmatrix} = \begin{pmatrix} f^{j-1} \\ \gamma^{j-1} \end{pmatrix} - \begin{pmatrix} \delta_f \\ \delta \end{pmatrix} \nabla_{f,\gamma} detA^{(N)}(f^{j-1}, \gamma^{j-1}), j = 1, 2, 3, \ldots, \tag{19}$$

where $\delta_f = \delta \cdot 10^{12}$ Hz, δ is the step, and j is the iteration's number. To calculate the gradient in Eq. (19), we use the finite-difference scheme. However, Eq. (19) represents an iterative procedure that heavily depends on the initial-guess approximation for the LEP eigenvalue pair, (f, γ). To determine the initial approximation, we build the color map of $|detA^{(N)}|$ on the (f, γ) plane. After that, we identify the minima of $|detA^{(N)}|$ on the relief and use them as the initial approximation for Eq. (19). The criterion to confirming that the located point, following Eq. (19), is the zero is the change in the sign of both real and imaginary parts of $detA^{(N)}$ upon passing through that point. As an example, we show such a map in Fig. 2.

Optics EXPRESS

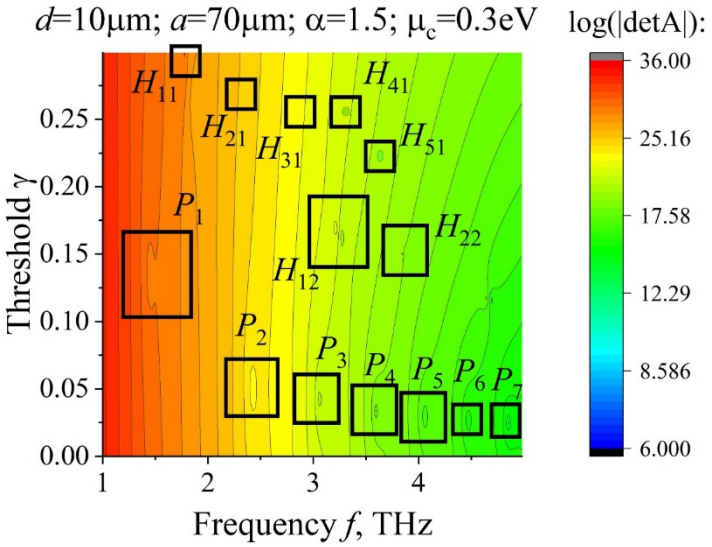

Fig. 2. Color map of $|detA^{(N)}|$ on the (f, γ) plane for the QWR and graphene strip parameters as indicated and the integral equation discretization order $N = 20$.

As already mentioned, the considered nanolaser consists of two open resonators: QWR and graphene strip. As a result, its natural modes form two families of different nature. One of them corresponds to the modes of QWR, which were double degenerate in the absence of strip and get perturbed or not perturbed by the presence of graphene strip. These modes remain if the strip vanishes. The other family corresponds to the plasmon modes of the graphene strip – they remain if QWR vanishes. This co-existence of modes is similar to the nanolaser built on the noble-metal strip inside the circular QWR, studied in [30]. We denote these modes as $H^{\pm}_{mn}$ and P_m, respectively.

Additionally, the considered nanolaser cross-section is symmetric with respect to the x-axis and the y-axis. Therefore, similar to the noble-metal counterpart in [30], it can support the modes of four orthogonal types of symmetry, EE, EO, OE and OO, where E (O) stands for the even (odd) mode field function of x and y. Here, it is obvious that the presence of the graphene strip is irrelevant to the modes the EE and OE types because the strip is zero-thickness and sits in the electric field zero. Hence, these mode types contain only the QWR modes H^{+}_{mj} with magnetic field depending on the azimuth as $\cos m\phi$. In contrast, the EO and OO types contain both the strip-perturbed quasi-H^{-}_{mj} modes of QWR, depending on azimuth as a series in $\sin m\phi$, and the plasmon modes P_m of the strip itself. Consequently, Eq. (14) can be split into two separate integral equations, which correspond to x-even, $w(x) = w(-x)$, and x-odd surface current, $w(x) = -w(-x)$, respectively, and studied independently.

The characteristics of the graphene strip plasmon modes *in homogenous medium* can be estimated analytically, by following the same lines as in [36] (Eq. (33)) and [33] (Eqs. (12) and (13)). Here, a plasmon mode is viewed as the mode of the 1-D Fabry-Perot resonator working on the graphene plasmon wave that bounces between the strip edges. The complex propagation constant of such wave has analytical description – see Appendix in [36]. Then, assuming that the frequency is not extremely high and the graphene conductivity is dominated by the intraband (Drude) term and, additionally, neglecting the radiation losses, the plasmon mode wavenumbers,

Optics EXPRESS

$k = 2\pi f/c$, and thresholds gain indices are obtained as

$$k_m^p \approx \frac{1}{2\alpha}\left[\frac{\pi(m-0.25)\Omega}{cd}\right]^{1/2}, \quad \gamma_m^p \approx \frac{2\alpha^2}{\tau}\left[\frac{d}{\pi(m-0.25)\Omega c}\right]^{1/2}, \tag{20}$$

where

$$\Omega = \frac{q_e^2 k_B T Z_0}{\pi\hbar^2}\left\{\frac{\mu_c}{k_B T} + 2\ln\left[1 + exp\left(-\frac{\mu_c}{k_B T}\right)\right]\right\}, \tag{21}$$

q_e is the electron charge, k_B is the Boltzmann constant, and $\hbar$ is the reduced Planck's constant.

In [33] and [36], the authors compare the frequency given by Eq. (20) with the results of the full-wave modeling. They show that although these expressions are approximate, their accuracy is good and even better than could be expected. Equation (20) can be also taken as initial-guess approximations for the LEP eigenvalue pairs in the iterative search algorithm.

Expressions (20) and (21) show that, similar to the graphene nanotube laser case [33], the product of the plasmon-mode wavenumber and the threshold gain index (used in the laser theories as "gain per wavelength" quantity) does not depend on the mode number (index m), the strip width $2d$, and the graphene chemical potential μ_c. It is determined by α and τ as follows:

$$k_m^p \cdot \gamma_m^p = \frac{\alpha}{c\tau}. \tag{22}$$

Note that in the case of the configuration shown in Fig. 1, the graphene-strip cavity is not in the homogeneous medium but inside a circular QWR of finite radius, a. Therefore, the agreement with Eq. (22) is expected to become better if a gets significantly larger than d.

4. Numerical results

Before presenting the results of the numerical analysis of the threshold conditions for the modes of considered nanolaser, we study the convergence of Eq. (19) with respect to the number of iterations. All results presented below are obtained for the discretization order $N = 20$. The number of terms taken into account in sums in (10) is 20. This is because the verification has shown that doubling the N leads to changes in the results at the 6-th decimal place. Figure 3 shows dependences of $|detA^{(N)}|$ on the number of iterations for two cases: δ is constant and δ is adaptively changed. As one can see, the convergence is not monotonic. If δ is constant, starting from a certain number of iterations, $|detA^{(N)}|$ shows oscillations with not decreasing amplitude. Therefore, we use the following approach: if $|detA^{(N)}|$ starts increasing, we decrease δ ten-fold – this guarantees that the determinant keeps going down.

Figures 4, 5, and 6 show the trajectories of the modes, i.e. the LEP eigenvalues, as solutions of Eq. (16), on the (f, γ) plane under the variation of the chemical potential, in the frequency range from 0 to 5 THz. The values of the graphene chemical potential vary from 0.1 eV to 1 eV (which is the largest accessible today value, according to the publications [37,38]) with the step of $\Delta\mu_c = 0.1$eV. The temperature is $T = 300$ K and the electron relaxation time is $\tau = 1$ ps.

The results shown in Fig. 4 correspond to the microsize strip, $d = 10\,\mu$m and relatively thick QWR, of the large radius $a = 70\,\mu$m. The strip width $2d$ here is 7 times smaller than the QWR diameter. This results in the downshift of the frequencies of the QWR modes, H_{mn}^-, many of which are found below 5 THz and hence compete with the lower plasmon modes, P_m. With the parameters considered in Fig. 4, the threshold values of the higher-order plasmon modes, P_m, m>2, are smaller than the threshold values of the lower H_{mn}^- modes, which have large radiation losses. The same is true for the first plasmon mode P_1, however, only if the chemical potential is smaller than μ_c<0.45 eV. This is because around that value the P_1 frequency approaches the frequency of the lowest mode of QWR of the same symmetry, H_{11}^-, and two modes hybridize. As usual, hybridization leads to the growth of one mode threshold and the drop of the other.

Optics EXPRESS

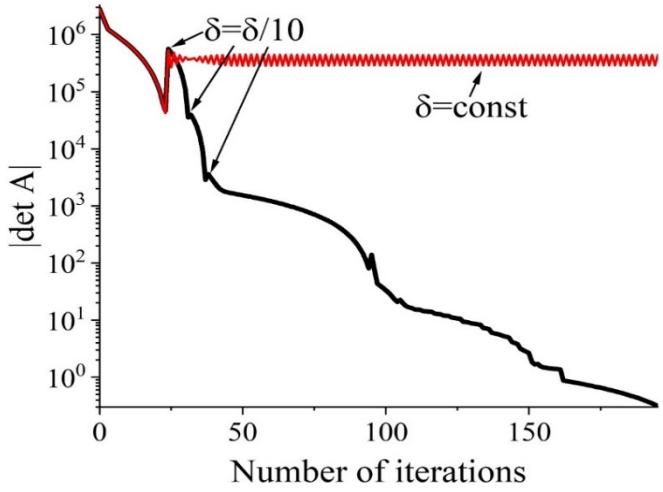

Fig. 3. Dependences of $|detA^{(N)}|$ on the number of iterations in (19) for the same set of parameters as in Fig. 2. Integral equation discretization order is $N = 20$.

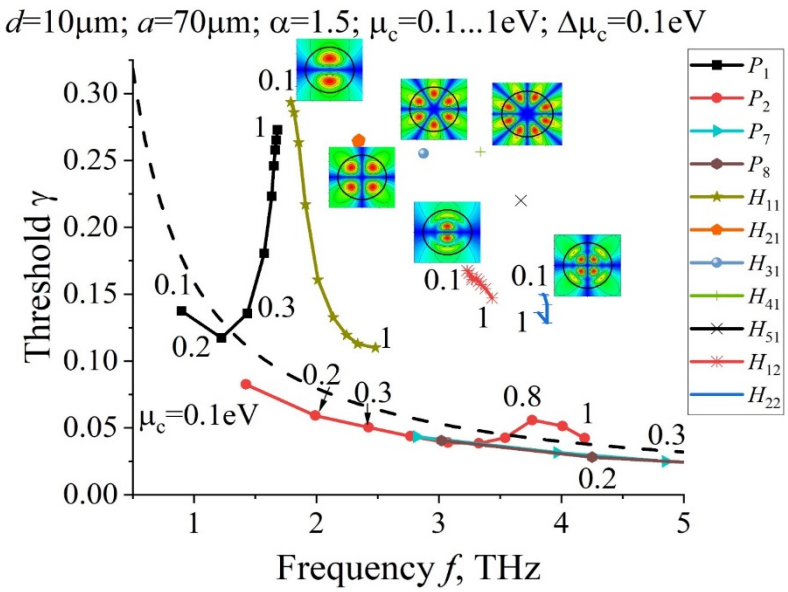

Fig. 4. Mode trajectories on the plane (f, γ) for varying chemical potential $\mu_c \in [0.1, 1]$ eV with the step $\Delta\mu_c = 0.1$eV, and $d = 10$ μm, $a = 70$ μm, $\alpha = 1.5$. Some of the values of the chemical potential are indicated near the trajectories. The hyperbolic curve defined by (20) is shown as dashed line. Insets demonstrate the near field patterns, in the area 90 μm × 90 μm, of the QWR modes H^{-}_{mj} at $\mu_c = 0.1$ eV (superscript "–" is omitted in Figure). The black circle illustrates the boundary of QWR, while a white box corresponds to the strip.

Optics EXPRESS

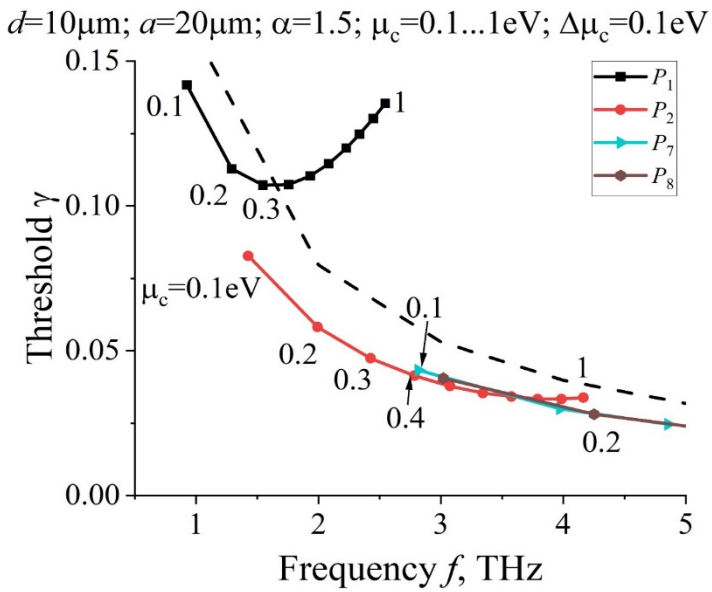

Fig. 5. The same study as in Fig. 3, however, for $a = 20\mu m$.

For the smaller values of the QWR radius a, the natural frequencies of the QWR modes H_{mj} get larger as $O(m/a)$ and hence shift away from the plasmon-mode frequencies, which get larger as well, however, less rapidly, as $O\left(\sqrt{m/d}\right)$ - see (20). Thus, for $a = 20\mu m$ (the case of Figs. 5 and 6), the natural frequency of the H_{11}^{-} mode is approximately equal to 6.25 THz for $\mu_c = 0.1$ eV. Increasing the width of the strip leads to the downshift of the natural frequencies of the plasmon modes, as predicted by (20), while increasing the chemical potential leads to their upshift proportionally to $O\left(\sqrt{\mu_c}\right)$.

The hyperbolic curve defined by Eq. (22) is shown in Figs. 4, 5, and 6 as dashed line. As visible, the LEP eigenvalues follow the trajectories that agree with Eq. (22), however, pass below that curve. This is understandable because the finite radius of QWR can be understood as the factor, lowering the effective refractive index, α. Indeed, if $a>>d$, the agreement with Eq. (22) becomes better.

To identify the modes, we study their field patterns. Figure 7 shows the magnetic near and far field portraits of several plasmon and QWR modes. The parameters correspond to Fig. 4, while $\mu_c = 0.1$eV that is the value of the chemical potential that is far from the hybridization and all the modes are easily identifiable.

The near fields of the plasmon modes are concentrated near the surface of the graphene strip and their amplitudes decrease quickly with the distance from the strip. The fields of the quasi-QWR modes H_{mn}^{-} stretch far beyond the QWR boundary that indicates high level of radiation losses. The numbers of the field variations along the strip width and along the QWR circumference and radius correspond to the mode indices.

As predicted by Eq. (20), the plasmon modes natural frequencies are well tunable under the variation of the graphene chemical potential. However, in certain frequency ranges the natural frequencies of the lowest QWR modes also show stronger dependence on the chemical potential that is an indication of their hybridization with the plasmon modes. In Fig. 4, this is clearly seen for the modes P_1 and H_{11}^{-} around 1.9 THz as well as for the P_2 and H_{22}^{-} modes around 3.9 THz. Due to hybridization, the thresholds of the plasmon modes increase, while those of the perturbed QWR modes drop.

Optics EXPRESS

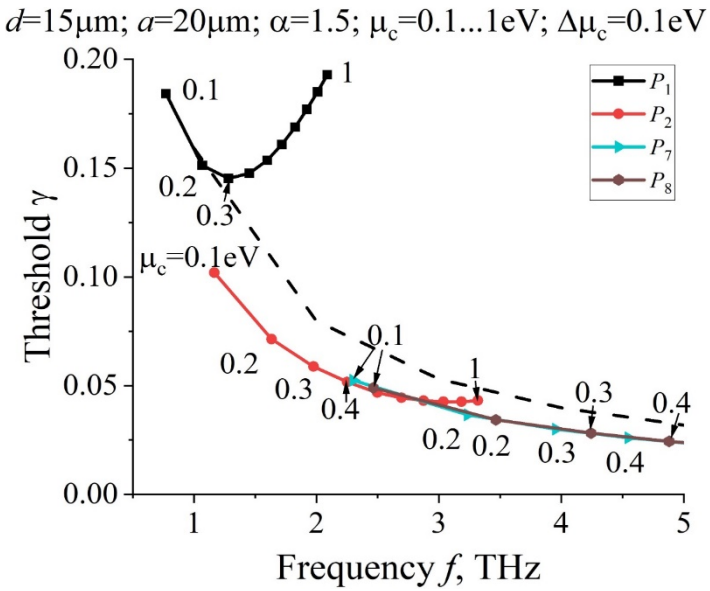

Fig. 6. The same study as in Fig. 5, however, for $d = 15\mu m$.

The growth of the thresholds of the P_1 mode is observed also in Figs. 5 and 6, however, here it is not connected with hybridization and is not as pronounced as in Fig. 4. The near magnetic field patterns of the P_1 and H_{11}^- modes for two values of the chemical potential are presented in Fig. 8.

The maxima of the field absolute value are observed near the graphene strip as well as away from the strip however inside QWR (compare with Fig. 7). Note that the panels computed for $\mu_c = 1$ eV demonstrate that the hybridizing modes have already exchanged their field patterns – the plasmon mode field looks like the QWR mode field at 0.4 eV and vice versa.

Finally, Fig. 9 shows the trajectories of the plasmon modes on the plane (f, γ) for the nanosize graphene strip with $d = 50$ nm inside the relatively thick QWR of the radius $a = 1$ μm so that $a/d = 20$.

For such a narrow strip, the plasmon mode frequencies are upshifted to the range from 10 THz to 65 THz, and the QWR modes are blue-shifted even further, off the considered frequency range. The trajectories correspond to the graphene chemical potential variation from 0.1 eV to 1 eV with the step of $\Delta\mu_c = 0.1$ eV. Similar to the microsize strip, the plasmon mode natural frequencies exhibit growth with increasing chemical potential. The essential difference is that at small values of the chemical potential, the thresholds of the higher plasmon modes exceed the thresholds of the lowest plasmon modes. For example, at $\mu_c = 0.1$eV we have $\gamma_1^p < \gamma_2^p < \gamma_3^p \ldots$.

As mentioned in Introduction, it is interesting to compare the threshold characteristics for the modes of the laser made of QWR center-loaded with a graphene strip and the same QWR with a silver strip, considered using LEP in [30]. Inspection of Fig. 9 and Figs. 3 and 4 of [30] shows that, apart of the different frequency ranges, the threshold values of the gain index are by order lower in the case of the graphene plasmonic nanolaser. This is apparently explained by the lower losses in the graphene as material than in silver. In [33], the wire was fully coated with graphene, so that only one side of the plasmon cavity touched the active region. In contrast, in our work the strip is embedded into the active material. Thanks to this, with comparable graphene element sizes, the threshold gain values for the plasmon modes become approximately twice lower because of the better overlap between the mode electric field and the active region [25]. This holds true for the case where hybridization with the H_{mn}-modes does not occur.

Optics EXPRESS

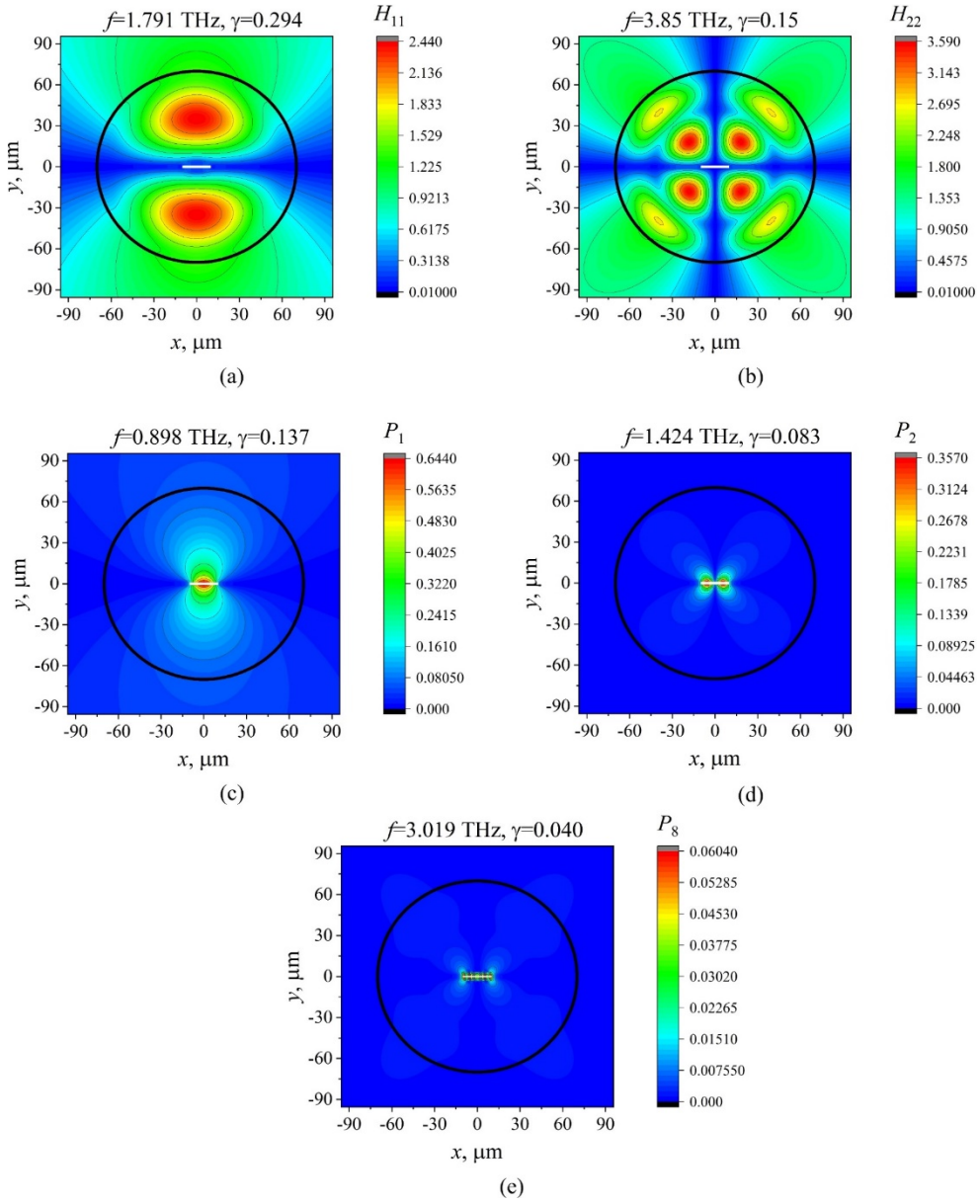

Fig. 7. Near magnetic field patterns of the perturbed QWR modes (a), (b) and plasmon modes (c), (d), (e) at μ_c = 0.1eV, $d = 10\mu m$, $a = 70\mu m$, α = 1.5.

Optics EXPRESS

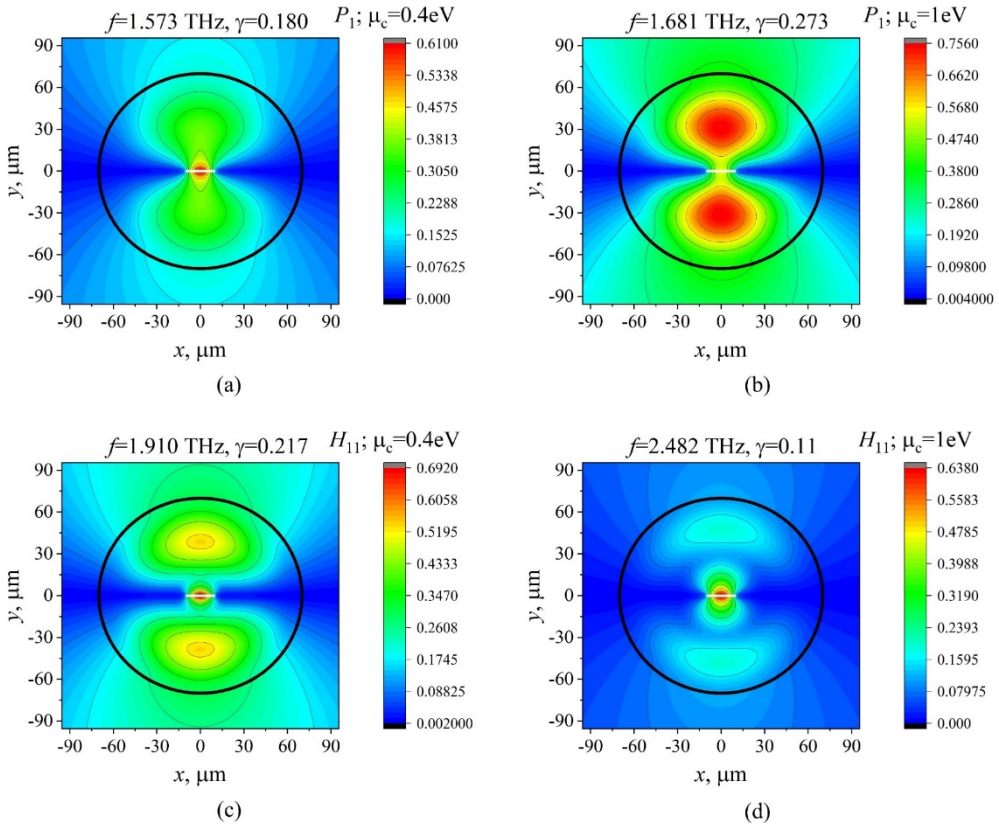

Fig. 8. Comparison of the near magnetic field patterns of the P_1 and H_{11}^{-} modes just below and just above the hybridization band of Fig. 4, at μ_c = 0.4eV (a), (c) and μ_c = 1eV (b), (d), $d = 10\mu m$, $a = 70\mu m$, $\alpha = 1.5$.

Single-mode operation is typically preferred for nanolaser applications. For the considered parameters, the first plasmon mode is the most promising one, and the number of modes can be regulated by adjusting the pumping power. If the pumping power falls below the threshold condition of a particular mode, that mode remains dark. Working mode selection can be also controlled by the choice of the gain material because each material has a specific frequency envelope of the gain.

Optics EXPRESS

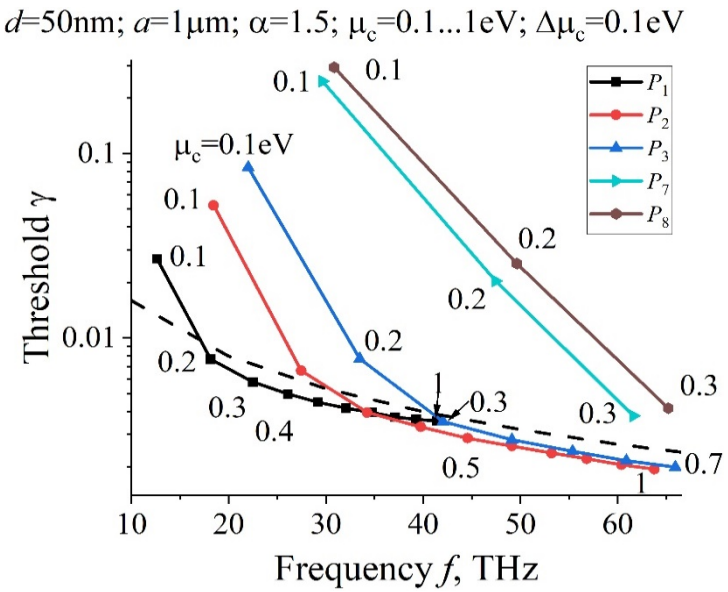

Fig. 9. Trajectories on the plane (f, γ) for the chemical potential varying from 0.1 eV to 1 eV with the step $\Delta\mu_c = 0.1$ eV, for $d = 50nm$, $a = 1\mu m$, $\alpha = 1.5$. The values of the chemical potential are indicated.

5. Conclusions

We have presented the results of the threshold conditions analysis of the plasmonic micro/nano laser based on the circular QWR symmetrically loaded with the graphene strip. In this analysis, our computational instrument is the full-wave LEP approach, which is tailored to deliver not only the mode-specific emission frequencies but also the threshold values of the gain in the active region. We have cast the LEP to a hypersingular boundary integral equation for the strip current function and discretized it using the Nystrom-type technique – this algorithm has mathematically guaranteed convergence and avoids the need for structured grids. Therefore, it is reliable and computationally efficient. The real-valued natural frequencies and the corresponding threshold gain index values are two-component zeros of the determinant of the matrix, obtained after discretization. If desired, our algorithm allows to obtain the results with machine precision.

As we have found, the natural frequencies of the plasmon modes are well tunable by the variation of the chemical potential of graphene, so that the mode frequency can double or triple when the potential changes from 0.1 eV to 1 eV. If the QWR is relatively thin, i.e. its diameter is slightly larger than the strip width, then the lowest plasmon modes have much lower frequencies and thresholds than the modes of QWR, perturbed by the strip. However, if QWR is relatively thick, i.e. much wider than the strip, then the corresponding natural frequencies and thresholds are comparable. In this case, the variation of the graphene chemical potential can lead to the hybridization between a plasmon mode and a QWR-mode of the same symmetry type. In the case of the nanosize strip of graphene, the thresholds of the lowest plasmon modes are by order lower than those of the similar QWR loaded with a silver nanostrip.

Funding. National Research Foundation of Ukraine (2020.02.0150); Ministry of Education and Science of Ukraine (0122U001436, 0122U001486, 0124U000670).

Acknowledgment. O.I.N. acknowledges support of the European Federation of Academies of Sciences and Humanities via the European Fund for Displaced Scientists and the Institute of International Education's Scholar Rescue Fund.

Optics EXPRESS

Disclosures. The authors declare no conflicts of interest.

Data availability. The authors have presented the equations, which can be directly programmed by the reader, delivering all the results reported in the paper.

References

1. S. I. Azzam, A. V. Kildishev, R.-M. Ma, *et al.*, "Ten years of spasers and plasmonic nanolasers," Light: Sci. Appl. **9**(1), 90 (2020).
2. M. H. Huang, S. Mao, H. Feick, *et al.*, "Room-temperature ultraviolet nanowire nanolasers," Science **292**(5523), 1897–1899 (2001).
3. X. Duan, Y. Huang, R. Agarwal, *et al.*, "Single-nanowire electrically driven lasers," Nature **421**(6920), 241–245 (2003).
4. A. H. Chin, S. Vaddiraju, A. V. Maslov, *et al.*, "Near-infrared semiconductor subwavelength-wire lasers," Appl. Phys. Lett. **88**(16), 163115 (2006).
5. A. V. Maslov and C. Z. Ning, "Far-field emission of a semiconductor nanowire laser," Opt. Lett. **29**(6), 572–574 (2004).
6. S. W. Eaton, A. Fu, A. B. Wong, *et al.*, "Semiconductor nanowire lasers," Nat. Rev. Mater. **1**(6), 16028 (2016).
7. A. V. Maslov and C. Z. Ning, "Size reduction of a semiconductor nanowire laser by using metal coating," Phys. Simul. Optoelectron. Devices XV **6468**, 64680I (2007).
8. M. T. Hill, M. Marell, E. S. P. Leong, *et al.*, "Lasing in metal-insulator-metal sub-wavelength plasmonic waveguides," Opt. Express **17**(13), 11107–11112 (2009).
9. R. F. Oulton, V. J. Sorger, T. Zentgraf, *et al.*, "Plasmon lasers at deep subwavelength scale," Nature **461**(7264), 629–632 (2009).
10. M. A. Noginov, G. Zhu, A. M. Belgrave, *et al.*, "Demonstration of a spaser-based nanolaser," Nature **460**(7259), 1110–1112 (2009).
11. R.-M. Ma, R. F. Oulton, V. J. Sorger, *et al.*, "Room-temperature sub-diffraction-limited plasmon laser by total internal reflection," Nat. Mater. **10**(2), 110–113 (2011).
12. R.-M. Ma, X. Yin, R. F. Oulton, *et al.*, "Multiplexed and electrically modulated plasmon laser circuit," Nano Lett. **12**(10), 5396–5402 (2012).
13. Q. Zhang, G. Li, X. Liu, *et al.*, "A room temperature low-threshold ultraviolet plasmonic nanolaser," Nat. Commun. **5**(1), 4953 (2014).
14. S. Wang, B. Li, X.-Y. Wang, *et al.*, "High-yield plasmonic nanolasers with superior stability for sensing in aqueous solution," ACS Photonics **4**(6), 1355–1360 (2017).
15. Z. Wu, J. Chen, Y. Mi, *et al.*, "All-inorganic CsPbBr3 nanowire based plasmonic lasers," Adv. Opt. Mater. **6**(22), 1800674 (2018).
16. G. W. Hanson, "Dyadic Green's functions and guided surface waves for a surface conductivity model of graphene," J. Appl. Phys. **103**(6), 064302 (2008).
17. G. W. Hanson, "Dyadic Green's functions for an anisotropic, non-local model of biased graphene," IEEE Trans. Antennas Propag. **56**(3), 747–757 (2008).
18. M. Yasir, F. Peinetti, and P. Savi, "Enhanced graphene based electronically tunable phase shifter," Micromachines **14**(10), 1877 (2023).
19. R.-B. Hwang, "A theoretical design of evanescent wave biosensors based on gate-controlled graphene surface plasmon resonance," Sci. Rep. **11**(1), 1999 (2021).
20. W. Fuscaldo, P. Burghignoli, P. Baccarelli, *et al.*, "Efficient 2-D leaky-wave antenna configurations based on graphene metasurfaces," Int. J. Microw. Wireless Technol. **9**(6), 1293–1303 (2017).
21. M.-L. Zhai and D.-M. Li, "Tunable hybrid metal-graphene frequency selective surfaces based on split-ring resonators by leapfrog ADI-FDTD method," Micro Nano Lett. **13**(9), 1276–1279 (2018).
22. M. E. Kaliberda and S. A. Pogarsky, "Tunability of radiation pattern of the H-polarized natural waves of dielectric waveguide with infinite graphene plane and finite number of graphene strips at THz," Appl. Sci. **13**(19), 10563 (2023).
23. V. Apalkov and M. I. Stockman, "Proposed graphene nanospaser," Light: Sci. Appl. **3**(7), e191 (2014).
24. B. Liu, W. Zhu, S. D. Gunapala, *et al.*, "Open resonator electric spaser," ACS Nano **11**(12), 12573–12582 (2017).
25. E. I. Smotrova, V. O. Byelobrov, T. M. Benson, *et al.*, "Optical theorem helps understand thresholds of lasing in microcavities with active regions," IEEE J. Quantum Electron. **47**(1), 20–30 (2011).
26. V. O. Byelobrov, T. M. Benson, and A. I. Nosich, "Binary grating of sub-wavelength silver and quantum wires as a photonic-plasmonic lasing platform with nanoscale elements," IEEE J. Select. Topics Quantum Electron. **18**(6), 1839–1846 (2012).
27. E. I. Smotrova, V. Tsvirkun, I. Gozhyk, *et al.*, "Spectra, thresholds and modal fields of a kite-shaped microcavity laser," J. Opt. Soc. Amer. B **30**(6), 1732–1742 (2013).
28. E. I. Smotrova and A. I. Nosich, "Optical coupling of an active microdisk to a passive one: Effect on the lasing thresholds of the whispering-gallery supermodes," Opt. Lett. **38**(12), 2059–2061 (2013).
29. A. O. Spiridonov, E. M. Karchevskii, and A. I. Nosich, "Symmetry accounting in the integral-equation analysis of the lasing eigenvalue problems for two-dimensional optical microcavities," J. Opt. Soc. Am. B **34**(7), 1435–1443 (2017).

Optics EXPRESS

30. O. V. Shapoval, K. Kobayashi, and A. I. Nosich, "Electromagnetic engineering of a single-mode nanolaser on a metal plasmonic strip placed into a circular quantum wire," IEEE J. Select. Topics Quantum Electron. **23**(6), 1–9 (2017).
31. D.M. Natarov, T.M. Benson, and A.I. Nosich, "Electromagnetic analysis of the lasing thresholds of hybrid plasmon modes of a silver tube nanolaser with active core and active shell," Beilstein J. Nanotechnol. **10**, 294–304 (2019).
32. L. Prelat, M Cuevas, N. Passarelli, *et al.*, "Spaser and optical amplification conditions in graphene-coated active wires," J. Opt. Soc. Am. B **38**(7), 2118–2126 (2021).
33. D. O. Herasymova, S. V. Dukhopelnykov, D. M. Natarov, *et al.*, "Threshold conditions for transversal modes of tunable plasmonic nanolasers shaped as single and twin graphene-covered circular quantum wires," Nanotechnology **33**(49), 495001 (2022).
34. B. Ji, E. Giovanelli, B. Habert, *et al.*, "Non-blinking quantum dot with a plasmonic nanoshell resonator," Nat. Nanotechnol. **10**(2), 170–175 (2015).
35. J. M. Ortega and W. C. Rheinboldt, *Iterative solution of nonlinear equations in several variables* (Academic Press, 1970).
36. S.V. Dukhopelnykov, R. Sauleau, and A.I. Nosich, "Integral equation analysis of terahertz backscattering from circular dielectric rod with partial graphene cover," IEEE J. Quantum Electron. **56**(6), 1–8 (2020).
37. J. S. Gómez-Díaz and J. Perruisseau-Carrier, "Graphene-based plasmonic switches at near infrared frequencies," Opt. Express **21**(13), 15490–15504 (2013).
38. Y. Jeyar, K. Austry, M. Luo, *et al.*, "Casimir-Lifshitz force between graphene-based structures out of thermal equilibrium," Phys. Rev. B **108**(11), 115412 (2023).